THE JOURNAL OF BIOLOGICAL CHEMISTRY VOL. 282, NO. 15, pp. 11446–11455, April 13, 2007

The Molecular Basis of Glyphosate Resistance by an Optimized Microbial Acetyltransferase*

Received for publication, November 2, 2006, and in revised form, February 1, 2007 Published, JBC Papers in Press, February 1, 2007, DOI 10.1074/jbc.M610267200

Daniel L. Siehl[‡1,2], **Linda A. Castle**[‡], **Rebecca Gorton**[‡], **and Robert J. Keenan**[‡§1,3]

From [‡]*Pioneer Hi-Bred International, Redwood City, California 94063 and the* [§]*Department of Biochemistry and Molecular Biology, University of Chicago, Chicago, Illinois 60637*

GAT is an *N*-acetyltransferase from *Bacillus licheniformis* that was optimized by gene shuffling for acetylation of the broad spectrum herbicide, glyphosate, forming the basis of a novel mechanism of glyphosate tolerance in transgenic plants (Castle, L. A., Siehl, D. L., Gorton, R., Patten, P. A., Chen, Y. H., Bertain, S., Cho, H. J., Duck, N., Wong, J., Liu, D., and Lassner, M. W. (2004) *Science* 304, 1151–1154). The 1.6-Å resolution crystal structure of an optimized GAT variant in ternary complex with acetyl coenzyme A and a competitive inhibitor, 3-phosphoglycerate, defines GAT as a member of the GCN5-related family of *N*-acetyltransferases. Four active site residues (Arg-21, Arg-73, Arg-111, and His-138) contribute to a positively charged substrate-binding site that is conserved throughout the GAT subfamily. Structural and kinetic data suggest that His-138 functions as a catalytic base via substrate-assisted deprotonation of the glyphosate secondary amine, whereas another active site residue, Tyr-118, functions as a general acid. Although the physiological substrate is unknown, native GAT acetylates D-2-amino-3-phosphonopropionic acid with a k_{cat}/K_m of 1500 min^{-1} mM^{-1}. Kinetic data show preferential binding of short analogs to native GAT and progressively better binding of longer analogs to optimized variants. Despite a 200-fold increase in k_{cat} and a 5.4-fold decrease in K_m for glyphosate, only 4 of the 21 substitutions present in R7 GAT lie in the active site. Single-site revertants constructed at these positions suggest that glyphosate binding is optimized through substitutions that increase the size of the substrate-binding site. The large improvement in k_{cat} is likely because of the cooperative effects of additional substitutions located distal to the active site.

Glyphosate (*N*-phosphonomethylglycine) is a widely used herbicide that acts nonselectively through inhibition of 5-enolpyruvylshikimate-3-phosphate (EPSP)[4] synthase in the aromatic biosynthesis pathway (2). Its efficacy against all plant species, low cost, low mammalian toxicity, and benign environmental impact favor its use in crops that have a transgenic tolerance mechanism (3). The predominant transgene currently in use encodes a bacterial EPSP synthase that is nearly insensitive to inhibition by glyphosate (2). We reported an alternative strategy for glyphosate resistance involving enzymatic conversion of glyphosate to *N*-acetylglyphosate (NAG) (1). Because the acetylated form of glyphosate has low affinity for the active site of EPSP synthase, it is nonherbicidal. Three variants of an enzyme that catalyzes *N*-acetylation of the secondary amine of glyphosate were discovered from *Bacillus licheniformis*. These GAT[5] enzymes are 17 kDa in size, are most active at pH 6.8, and have a K_m for acetyl coenzyme A (AcCoA) of 1–2 μM. The native enzymes are very poor catalysts for acetylation of glyphosate, with a k_{cat} of 5.3 min^{-1} and $K_{m,GPJ}$ of 1.3 mM (for ST401 GAT, referred to hereafter as native GAT).[6] The *B. licheniformis* enzymes belong to a diverse family of largely uncharacterized bacterial *N*-acetyltransferases sharing between 30 and 64% amino acid identity to native GAT (Fig. 1). Despite extensive screening of biological amines, including amino acids, nucleotides and antibiotics, the physiological substrates for the native enzymes are unknown (4).

To develop *gat* as a transgene for glyphosate resistance in crops, we subjected the three *B. licheniformis* enzymes to 11 rounds of gene shuffling and obtained optimized variants with up to a 4,500-fold increase in catalytic efficiency (k_{cat}/K_m) relative to the native enzyme. This was achieved through a combination of improvements in k_{cat} (190-fold) and $K_{m,GPJ}$ (24-fold). When introduced into plants, optimized *gat* genes confer robust tolerance to glyphosate (1).

To gain insight into the molecular mechanism of glyphosate *N*-acetylation by GAT, we determined the structure of a 7th round GAT variant (termed R7 GAT) in ternary complex with AcCoA and the competitive inhibitor 3-phosphoglycerate (3PG) and in binary complex with oxidized CoA. We also car-

* The costs of publication of this article were defrayed in part by the payment of page charges. This article must therefore be hereby marked "*advertisement*" in accordance with 18 U.S.C. Section 1734 solely to indicate this fact.

The atomic coordinates and structure factors (code 2JDC, 2JDD) have been deposited in the Protein Data Bank, Research Collaboratory for Structural Bioinformatics, Rutgers University, New Brunswick, NJ (http://www.rcsb.org/).

[1] Both authors contributed equally to this work.

[2] To whom correspondence may be addressed. Tel.: 650-298-3556; Fax: 650-701-1258; E-mail: dan.siehl@pioneer.com.

[3] To whom correspondence may be addressed. Tel.: 773-834-2292; Fax: 773-702-0439; E-mail: bkeenan@uchicago.edu.

[4] The abbreviations used are: EPSP, 5-enolpyruvylshikimate 3-phosphate; GAT, glyphosate *N*-acetyltransferase; GNAT, GCN5-related *N*-acetyltransferase; AcCoA, acetyl coenzyme A; CoA, coenzyme A; GPJ, glyphosate; 3PG, 3-phosphoglycerate; NAG, *N*-acetylglyphosate; 3PG, 3-phosphoglyceric acid; AP3, 2-amino-3-phosphonopropionic acid; AP4, 2 amino-4-phosphonobutyric acid; AP5, 2-amino-5-phosphonopentanoic acid; PEP, phosphoenolpyruvate; AMPA, aminomethylphosphonate; r.m.s.d., root mean square deviation; PDB, Protein Data Bank.

[5] Optimum™ GAT™ is the trademark name that Pioneer Hi-Bred International, Inc., uses to identify its glyphosate ALS tolerance trait.

[6] The GenBank™ accession numbers for the sequences contained herein are as follows: *B. licheniformis* ST401 GAT, AX543338; R7 GAT, AY597417; R11 GAT, AY597418; *B. subtilis* YITI, CAA70664; *Bacillus cereus* GNAT, NP_830505; *Bdellovibrio bacteriovorus* GNAT, NP_967337; *Chloroflexus aurantiacus* GNAT, ZP_00018467; *Exiguobacterium sibiricum* GNAT, ZP_00538687; *Listeria inocua* GNAT, CAC98097.

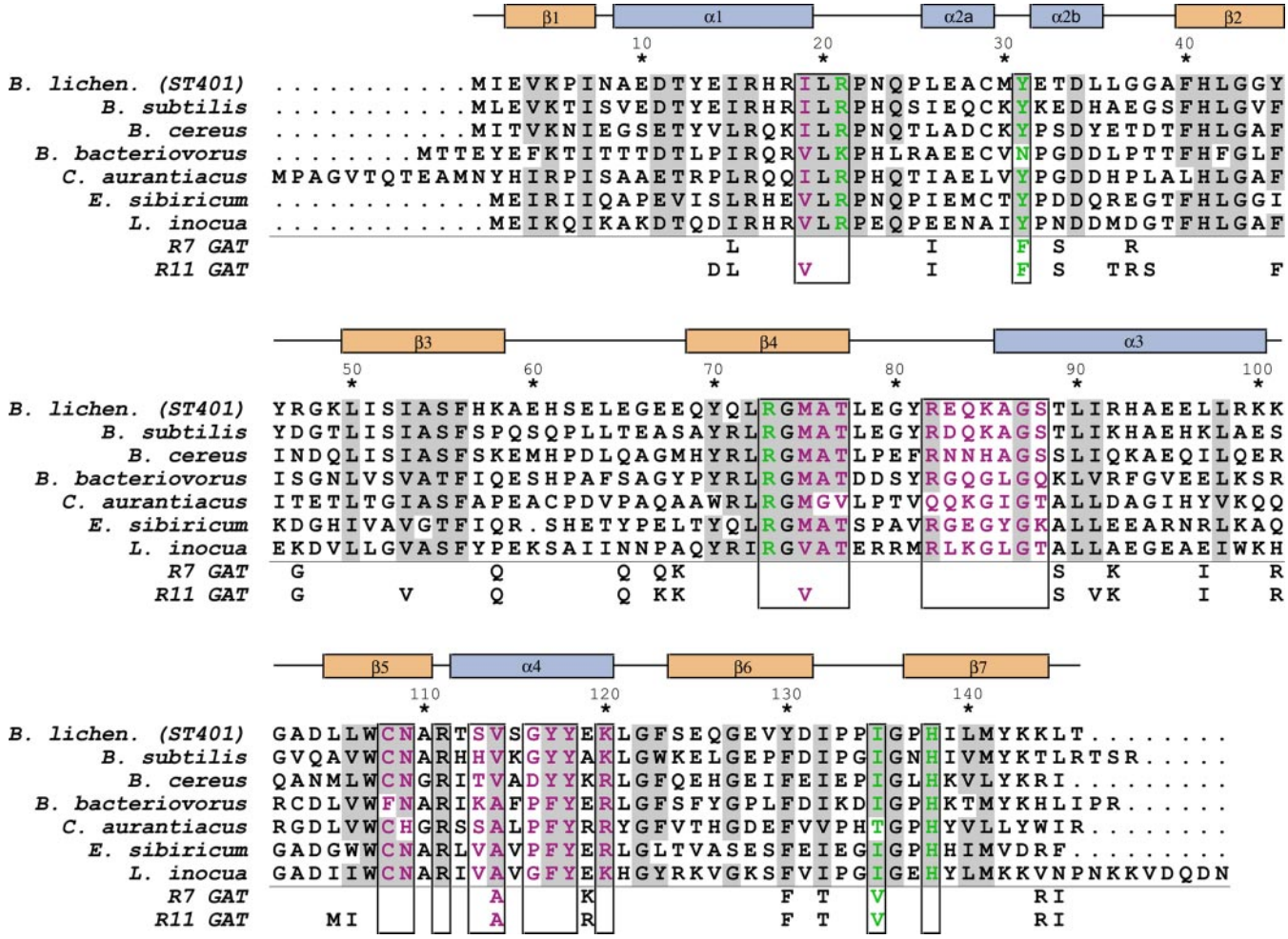

FIGURE 1. **Sequence alignment of *B. licheniformis* GAT (ST401) and six members of the GAT-like family of *N*-acetyltransferases.** These sequences share between 30 and 64% pairwise amino acid identity. The most conserved amino acids within the family are shaded *gray*. Amino acid differences between native GAT (ST401), seventh (R7), and eleventh (R11) round variants of GAT are indicated *below* the line. Secondary structure and numbering are shown for the R7 GAT sequence, colored as in Fig. 2*A*. Residues located within 4 Å of the cofactor (*magenta letters*), 3PG (*green letters*), or both (*black letters*) are *boxed*.

ried out a detailed kinetic analysis of the activity of native, optimized, and site-directed mutants of GAT against a panel of substrate analogs. Together, these data allow us to propose a detailed mechanism for glyphosate *N*-acetylation by GAT. Furthermore, comparison of the native and optimized enzymes provides insight into the structural basis of the activity enhancements achieved through gene shuffling.

EXPERIMENTAL PROCEDURES

General—Glyphosate, acetyl coenzyme A, coenzyme A, aminomethylphosphonate, glycine, *N*-methylglycine, 3-phosphoglycerate, phosphoenolpyruvate, DL-2-amino-4-phosphonobutyric acid, and DL-2-amino-5-phosphonopentanoic acid were obtained from Sigma. D- and L-2-amino-3-phosphonopropionic acids were purchased from American Radiolabeled Chemicals, St. Louis. *N*-Acetylglyphosate was synthesized by Gateway Chemical Technology, St. Louis. *N*-Methylaminomethylphosphonate was purchased from AKos Consulting, Basel, Switzerland. Phosphonoacetate was purchased from ICN Biomedicals, Aurora, OH. 4-Phosphonobutyrate was purchased from Lancaster Synthesis, Inc., Pelham, NH. Phosphonopyruvate was synthesized by Chemical Synthesis Services, Craigavon, UK.

Mutagenesis, Protein Expression, and Purification—Native and variant GAT enzymes were prepared as described (1). Briefly, *gat* genes were expressed in *Escherichia coli* from a pQE80 vector (Qiagen), modified to remove the His_6 tag. GAT was purified from cell lysates by affinity chromatography on coenzyme A-agarose (Sigma) and gel filtration chromatography on Superose 75 (Amersham Biosciences).

Site-directed mutagenesis of the R7 *gat* gene in pQE80 was performed using a QuikChange site-directed mutagenesis kit (Stratagene). Oligonucleotide pairs containing the substituted nucleotides were purchased from Operon Biotechnologies, Inc. All resulting plasmids were sequenced to verify that only the intended mutation was present in the coding region. Double mutants were obtained by successive application of the site-directed mutagenesis protocol.

Protein concentrations were calculated from measurements of absorbance at 205 nm ($E_{mg/ml} = 30.5$) after buffer exchange (NAP-5 column, Amersham Biosciences) into 50 mM Na_2SO_4. The extinction coefficient was determined by the procedure of Scopes (5), in which extinction, $cm^{-1}\ (mg/ml)^{-1} = 27 + 120(A_{280}/A_{205})$.

Kinetic Analysis—Apparent K_m values for glyphosate and the compounds in Table 3 were determined as described previously (4) in a continuous spectrophotometric assay in which cleavage of the thioester bond of AcCoA is monitored at 235 nm in a Spectramax Plus^{384} plate reader (Molecular Devices, Sunnyvale, CA). Reaction mixtures contained 25 mM Hepes, pH 6.8, 10% ethylene glycol, varied concentrations of acceptor substrate and saturating AcCoA (167 μM). The Spectramax software was programmed to convert change in absorbance to reaction velocity, μM/min, and to return parameters of the Lineweaver-Burk transformation of the Michaelis-Menten equation. The k_{cat} value was calculated from V_{max} and the concentration of GAT. The apparent K_m value for AcCoA was determined from initial rate measurements at saturating glyphosate, using mass spectrometric detection of NAG, as described (4), and the Lineweaver-Burk method.

The pH *versus* k_{cat} profiles were fit to the equation, $k_{cat,app} = k_{cat}/(1 + 10^{(pK1-pH)} + 10^{(pH-pK2)})$, where pK_1 is the dissociation constant for the ionizable group that promotes the reaction in its deprotonated form, and pK_2 is the dissociation constant of the ionizable group that promotes the reaction in its protonated form.

For R7 and R11 GAT, K_i values for the competitive inhibitors NAG, CoA, 3PG, and phosphoenolpyruvate were determined from slope re-plots of double-reciprocal plots in which AcCoA was fixed at 167 μM; the glyphosate was varied, and inhibitor was supplied at a selection of fixed concentrations. For native GAT, the K_i value for CoA was also determined as above. For all other enzyme and inhibitor combinations, K_i values were determined from a single concentration of inhibitor using the equation $K_{m,app} = K_m + K_m/K_i$ [I]. Inhibitor concentrations were as follows: 2 mM NAG, 50 μM 3PG, 10 μM phosphoenolpyruvate, 15 μM phosphonopyruvate with native GAT; 20 μM phosphonopyruvate with R7 and R11 GAT; and 5 μM phosphonoacetate and 2 mM phosphonobutyrate with all enzymes.

Crystallization and Data Collection—Purified R7 GAT was buffer-exchanged and concentrated to 10 mg/ml in 5 mM Hepes, pH 7.5. For crystallization the protein was incubated in the presence of 2 mM AcCoA alone or with 2 mM AcCoA and 20 mM 3PG. Crystals were obtained overnight by hanging drop vapor diffusion against a crystallization solution containing 100 mM NaOAc, pH 4.6, 150–300 mM ammonium sulfate, and 20–25% PEG4000. The crystals were mounted in nylon loops, after first transferring them to cryoprotectant comprising 100 mM NaOAc, pH 4.6, 25% PEG4000, and 20% glycerol supplemented with 2 mM AcCoA and 250 mM ammonium sulfate (binary complex) or 2 mM AcCoA, 50 mM 3PG, and 50 mM ammonium sulfate (ternary complex). Data were measured at 100 K at beamline 5.0.2 of the Advanced Light Source (ALS, Berkeley, CA) using an ADSC Q210 CCD detector. Although the crystals diffract to high resolution, as evidenced by the low R_{sym} and high $\langle I/\sigma I \rangle$ values in the highest resolution shell, the detector geometry limited the data collection to 1.6 Å. All data were processed using MOSFLM (6) and programs from the CCP4 suite (7). Data collection and refinement statistics are summarized in Table 1.

Structure Determination—The structures were determined by difference Fourier analysis using the isomorphous crystal structure of selenomethionine-substituted GAT (PDB entry 2BSW) (8) as the starting model, after removing ligands and water molecules, and applying a random positional displacement to all atoms. Inspection of initial $F_o - F_c$ difference maps revealed clear electron density for cofactor and 3PG in the ternary complex and cofactor and an active site sulfate ion in the binary complex. The electron density for the acetyl group of AcCoA in the ternary complex is weak, suggesting rotational disorder. The acetyl group was modeled (and subsequently refined) into the density in the chemically reasonable orientation in which its carbonyl oxygen points toward the backbone amides of Gly-74 and Met-75. There is also evidence for a minor (~30% occupancy) active site configuration in which 3PG is replaced by a sulfate ion and an additional water molecule. We did not observe convincing electron density for the acetyl group of AcCoA in the binary complex structure. Based on careful inspection of $F_o - F_c$ difference maps, we modeled the cofactor as oxidized CoA, although we cannot exclude the possibility that the bound species is AcCoA with a rotationally disordered acetyl group. No evidence for transfer of the acetyl group to the thiol of Cys-108 was observed, either kinetically or in the electron density maps of either structure. Refinement was carried out in REFMAC5 (9), and COOT (10) was used for model building. The use of anisotropic *B*-factors in the final stage of refinement was supported by a >1% drop in R_{free} and R_{cryst} for both data sets. All amino acids except for the N-terminal methionine, which is disordered, are included in the final models. PyMOL was used to generate all structure figures (11). Atomic coordinates and structure factors have been deposited in the PDB with accession numbers 2JDC (binary complex) and 2JDD (ternary complex).

TABLE 1
Crystallographic data collection and refinement statistics

	Binary complex	Ternary complex
Data collection		
Space group	*C*2	*C*2
Unit cell dimensions		
a, *b*, *c*	69.1, 48.9, 46.5 Å	69.8, 48.5, 46.8 Å
α, β, γ	90, 103.5, 90°	90, 103.6, 90°
Resolution range (Å)	32.2-1.6	45.6-1.6
Total/unique reflections	62,521/19,217	65,935/19,905
Completeness (%)[a]	96.0 (75.4)	98.7 (89.6)
$I/\sigma I$	47.9 (19.0)	41.1 (8.3)
R_{sym} (%)	2.3 (6.0)	2.6 (11.0)
Refinement and model statistics		
R_{cryst} (%)	14.8	15.5
R_{free} (%)	17.2	19.3
No. of atoms	1,349	1,373
Protein	1,164	1,177
Ligands/ions	54	62
Solvent	131	129
Average *B*-factor (Å^2)	14.0	16.0
Protein	12.8	14.9
Ligands/ions	16.7	17.1
Solvent	22.8	25.7
r.m.s. deviation from ideal		
Bond lengths (Å)	0.011	0.011
Bond angles (°)	1.5	1.5

[a] Values in parentheses are for the high resolution shell (1.66–1.60 Å).

RESULTS

Structural Overview of GAT

General Fold—We determined the 1.6-Å crystal structure of an optimized GAT (R7) in ternary complex with AcCoA and a

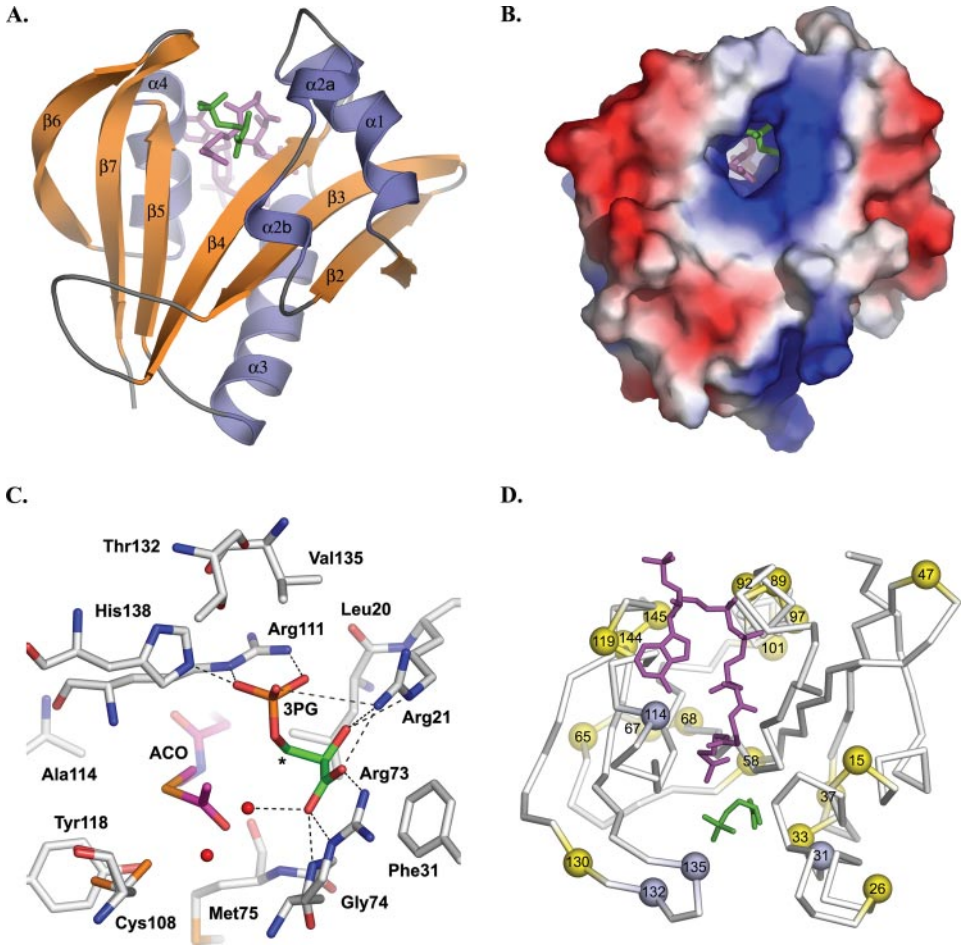

FIGURE 2. *A,* structure of R7 GAT bound to acetyl coenzyme A (*ACO*, *magenta*) and the competitive inhibitor, 3PG (*green*). *B,* molecular surface of the R7 GAT ternary complex colored by its electrostatic potential reveals the electropositive substrate-binding site. Acetyl coenzyme A and 3PG are shown in the active site cleft. *C,* close up of the active site. Polar contacts made by 3PG are indicated (*gray dashes*), and water molecules are shown as *red spheres.* Modeling glyphosate into the active site positions its 2° amine (equivalent position on 3PG marked with an *asterisk*) within 3.8 Å of the carbonyl carbon of AcCoA. *D,* shuffling changes are distributed throughout the enzyme. A C-α trace indicates the locations of 21 amino acid substitutions (*yellow* and *blue spheres*) made between native and R7 GAT. Substitutions located within 5 Å of either ligand are shown in *blue.*

competitive inhibitor, 3PG, and in binary complex with oxidized CoA (Table 1). Attempts to obtain a ternary complex with glyphosate were unsuccessful, presumably because of the low affinity of glyphosate for R7 GAT in the presence of ammonium sulfate, which was required for crystallization. GAT is a compact enzyme (Fig. 2*A*) with approximate dimensions of 43 × 40 × 38 Å. The crystal packing suggests that GAT functions as a monomer, in agreement with gel filtration results. Despite low primary sequence homology, the overall fold identifies GAT as a member of the GCN5-related *N*-acetyltransferase (GNAT) superfamily (12). GAT shows the closest structural similarity to YJCF (PDB code 1Q2Y; 19% sequence identity; 1.9 Å r.m.s.d.), a distantly related protein of unknown function from *Bacillus subtilis*, and more modest similarity to the well characterized aminoglycoside 6′-*N*-acetyltransferase Aac(6′)-Ii, (PDB code 1B87; 16% sequence identity; 2.7 Å r.m.s.d.) (13) and serotonin *N*-acetyltransferase (PDB code 1CJW; 14% sequence identity; 3.0 Å r.m.s.d.) (14).

Cofactor-binding Site—The interactions between cofactor and GAT are similar to those observed throughout the GNAT superfamily (15, 16). The adenosine group of AcCoA, which makes few direct interactions with the protein, is largely solvent-exposed, whereas the pyrophosphate and pantetheine moieties form a series of direct and water-mediated hydrogen bonds to the enzyme.

3PG-binding Site—The competitive inhibitor, 3PG, binds in a solvent-exposed cleft adjacent to the cofactor and the V-shaped wedge formed by β4 and β5. The binding site is flanked on one side by the region extending from the C-terminal portion of α1 into α2b and on the other side by the β6–β7 loop (Fig. 2*A*). These flanking regions are among the least conserved structural features within the GNAT superfamily, a reflection of the fact that these enzymes bind to a diverse set of substrates. The binding site is positively charged and surrounded by an otherwise electronegative surface (Fig. 2*B*). A total of 8 amino acids, 1 water molecule, and the acetyl group of AcCoA interact directly (<4 Å) with the inhibitor (Fig. 2*C*). The hydrophobic side chains of Leu-20, Phe-31, and Val-135 all contact 3PG, as does the main chain nitrogen of Gly-74, which forms a hydrogen bond with the carboxylate of 3PG. The majority of contacts, however, are made between charged groups, including side chain interactions with the phosphate end (Arg-21, Arg-111, and His-138) and with the carboxylate end (Arg-21 and Arg-73) of 3PG. Of particular note is a short, 2.46-Å hydrogen bond between the N-ϵ of His-138 and a phosphate oxygen of 3PG.

In contrast with the conformation observed in the binary complex, which contains a sulfate ion bound in the substrate-binding site, residues in the β6–β7 loop are displaced by up to 1.5 Å away from the active site in the ternary complex. This loop possesses the highest average *B*-factors in the ternary complex structure. In addition, side chains of residues lining the opposite face of the binding site, including Arg-21 and Arg-73, are displaced by up to 1.3 Å away from the active site to accommodate 3PG binding.

Certain features of the GAT structure appear to link the substrate- and cofactor-binding sites. Three well ordered water molecules are buried at the interface where α1, α2a, and α2b pack against the central β-sheet (Fig. 2*A*). The most deeply buried of these waters makes a series of hydrogen bonds to residues from three distinct regions of the enzyme: Arg-16,

TABLE 2
Steady-state kinetic data for native, R7, and R11 GAT enzymes, obtained as described under "Experimental Procedures"

Enzyme	k_{cat}	$K_{m,GPJ}$	$K_{i,NAG}$	$K_{m,AcCoA}$	$K_{i,CoA}$	$k_{cat}/K_{m,GPJ}$	Relative activity
	min^{-1}	mM	mM	μM	μM	$mM^{-1}\ min^{-1}$	
Native	5.3 ± 0.1	1.3 ± 0.1	1.3 ± 0.1	1.3 ± 0.1	13 ± 1	4.08	1.0
R7	1040 ± 40	0.24 ± 0.01	0.35 ± 0.03	1.5 ± 0.1	9 ± 1	4330	1060
R11	1010 ± 40	0.055 ± 0.004	0.06 ± 0.01	~1–2	15 ± 3	18400	4510

located at the C-terminal end of α1; Ser-55, located in the center of β3; and the backbone carbonyl of Gly-74, located in the β-bulge region of β4. Ser-55 is conserved in the GAT-like family of *N*-acetyltransferases, as is Arg-16, which forms a buried salt bridge with another conserved residue Asp-34 (on α2b). The proximity of these residues to the cofactor- (Gly-74) and substrate-binding sites (Leu-20, Arg-21, Phe-31, Arg-73, and Gly-74) suggests that the network of hydrogen bonds formed between β3, β4, α2a, and α2b is required for optimal binding of both ligands. Indeed, substitution of Asp34 with alanine in an 8th round GAT variant decreased K_m values for both AcCoA and glyphosate by 44- and 13-fold, respectively (data not shown).

Cofactor and Substrate Specificity for Native GAT and Optimized Variants

The steady-state kinetic parameters of native and optimized GAT enzymes used in this study are summarized in Table 2.

Cofactor Specificity—To characterize cofactor specificity, we compared the ability of GAT to utilize different acyl-CoAs for glyphosate *N*-acetylation. As reported previously, no activity was observed when 1 mM of the malonyl, crotonyl, succinyl, or 3-hydroxy-3-methylglutaryl derivatives of coenzyme A were incubated with 5 mM glyphosate and either native or R7 GAT (4). In contrast, activity was detected with propionyl-CoA and R7, and the following kinetic constants were determined: k_{cat} = 350 min^{-1}, $K_{m,PrCoA}$ = 100 μM, k_{cat}/K_m = 3.5 $min^{-1}\ \mu M^{-1}$. The corresponding values for AcCoA are 1040 min^{-1}, 1.5 μM, and 690 $min^{-1}\ \mu M^{-1}$. Thus, k_{cat}/K_m values with propionyl-CoA is only 0.5% that with AcCoA. This strict specificity is consistent with a lack of space in the active site for CoA derivatives with acyl groups appreciably larger than acetyl.

Acceptor Substrate Specificity—To define the range of sizes and functional groups that are preferred in substrates utilized by native, R7, and R11 GAT, we tested a series of compounds related to glyphosate (Table 3). Aminomethylphosphonate (AMPA), a glyphosate analog lacking a carboxyl group, was acetylated with nearly the same k_{cat} value as glyphosate by the native, R7, and R11 enzymes, but its K_m values are much higher than those of glyphosate. Relative to glyphosate, the K_m value for AMPA is 3.6-fold greater with native GAT, 17-fold greater with R7, and 133-fold greater with R11. Interestingly, *N*-methyl-AMPA had K_m values similar to those of AMPA, but k_{cat} values were 27- to 50-fold lower, suggesting steric hindrance from the methyl group. Glycine and *N*-methylglycine (sarcosine) were tested to probe the effect of removing the phosphonate group from glyphosate. Even when supplied at 100 mM, essentially no activity was observed with any of the three GAT variants. The contrasting effects obtained from removal of the phosphonate group compared with removal of the carboxyl group show that the former provides more binding energy for catalysis with glyphosate.

The only compound we tested that was acetylated appreciably by native GAT was D-2-amino-3-phosphonopropionate (D-AP3), exhibiting a k_{cat}/K_m of 1500 $min^{-1}\ mM^{-1}$. Activity with D-AP3 was less with R7 and R11 (Table 3). Activity with the L-isomer was very poor with the native enzyme and almost undetectable with the optimized variants. The DL form of the next longer compound, DL-2-amino-4-phosphonobutyrate (DL-AP4), showed only slight activity at 100 mM with all enzymes, and the longest, DL-2-amino-5-phosphonopentanoate (DL-AP5), was devoid of reactivity (see below).

We also tested a series of compounds for their ability to inhibit glyphosate *N*-acetylation (Table 3). NAG inhibited each enzyme competitively with glyphosate. K_i values decreased in parallel with $K_{m,GPJ}$ and were 1.3 mM (native), 0.35 mM (R7), and 0.06 mM (R11). Despite being a poor substrate, L-AP3, was a potent inhibitor of both R7 and R11, with K_i values of 5 and 10 μM, respectively (Table 3). The next longer compound, DL-AP4, was a poor inhibitor of native GAT but bound 53-fold more tightly to R11 than to native GAT. The longest compound, DL-AP5, did not inhibit native GAT and only weakly inhibited R7 and R11. A similar trend was observed with the competitive inhibitors 3PG and phosphoenolpyruvate (PEP). The shorter of the two compounds, PEP, showed lower K_i values than 3PG for native, R7, and R11, but the fold difference decreased throughout the optimization as follows: 12-fold tighter with the native enzyme, 5.3-fold with R7, and only 2.4-fold with R11. Similar results were obtained with the PEP analog, phosphonopyruvate. The shortest compound tested, 2-phosphonoacetate was a potent inhibitor of the native, R7, and R11 enzymes.

Kinetic Analysis of Site-directed Mutants

Glyphosate Binding—In the crystal structure of R7 GAT bound to AcCoA and 3PG, there are 8 residues located within 4 Å of the inhibitor. To examine the role of these residues in binding to glyphosate, we constructed a series of point mutants in R7 GAT and determined their kinetic parameters (Table 4). Mutation of Arg-111, Arg-73, or Arg-21 to alanine resulted in a 170–250-fold increase in $K_{m,GPJ}$. Likewise, a significant increase in glyphosate K_m was observed for H138A (44-fold) and the more conservative L20I (32-fold) mutant.

Enzyme Mechanism—To probe the mechanism of glyphosate *N*-acetylation by GAT, we characterized the kinetic parameters for the native enzyme and optimized variants, as well as for site-directed mutants constructed in R7 GAT. The structure reveals a conserved cysteine in the active site (Cys-108) that assumes alternate conformations within the crystal. In the conformation pointing toward the active site, the cysteine sulf-

TABLE 3

Substrate specificity of native, R7 and R11 GAT, performed as described under "Experimental Procedures"

"None" means that activity at a compound concentration of 10 mM was below the detection limit (LOD 90% = Blank AVE + 3(Blank SD); typically ~1 μM/min). "Trace" means that activity was above the LOD but insufficient for kinetic analysis.

Compound	Structure	Enzyme	k_{cat}	K_m	k_{cat}/K_m	K_i
			min^{-1}	mM	$mM^{-1}\ min^{-1}$	mM
Glyphosate (GPJ)	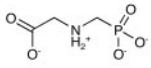	Native	5.3	1.3	4.08	
		R7	1040	0.24	4330	
		R11	1010	0.055	18400	
N-acetylglyphosate (NAG)	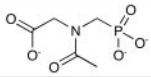	Native				1.3
		R7				0.35
		R11				0.06
Aminomethylphosphonate (AMPA)	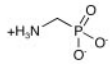	Native	12	4.7	2.6	
		R7	1000	4.0	250	
		R11	1600	7.3	220	
N-methyl-aminomethylphosphonate	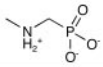	Native	Trace			
		R7	37	5.3	7.0	
		R11	32	3.9	8.2	
Glycine	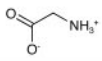	Native	None			
		R7	None			
		R11	Trace			
N-methylglycine (Sarcosine)		Native	None			
		R7	None			
		R11	Trace			
L-2-Amino-3-phosphonopropionate (L-AP3)	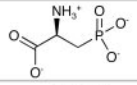	Native	13	2.3	5.7	
		R7	Trace			0.005
		R11	Trace			0.010
D-2-Amino-3-phosphonopropionate (D-AP3)	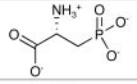	Native	660	0.44	1500	
		R7	27	0.25	110	
		R11	150	0.45	330	
DL-2-Amino-4-phosphonobutyrate (DL-AP4)	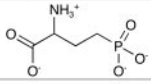	Native	Trace			30
		R7	Trace			1.9
		R11	Trace			0.57
DL-2-Amino-5-phosphonopentanoate (DL-AP5)	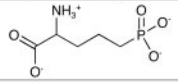	Native	None			No inhibition
		R7	None			34
		R11	None			5.5
4-Phosphonobutyrate	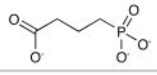	Native				0.93
		R7				0.99
		R11				0.57
2-Phosphonoacetate	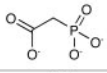	Native				0.009
		R7				0.001
		R11				0.003
D-3-Phosphoglycerate (3PG)	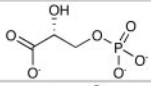	Native				0.14
		R7				0.042
		R11				0.022
Phosphoenolpyruvate (PEP)	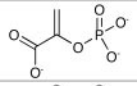	Native				0.012
		R7				0.008
		R11				0.009
Phosphonopyruvate	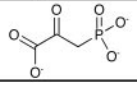	Native				0.011
		R7				0.025
		R11				0.021

hydryl is located 3.8 Å from the carbonyl carbon of AcCoA (Fig. 2*C*). To clarify the role of this cysteine in catalysis, we substituted it with alanine in R7 GAT. The resulting enzyme was fully active with glyphosate (Table 4). Reaction with the sulfhydryl reagent 5,5′-dithiobis-2-nitrobenzoate inactivated any variant with Cys-29 present, as well as C108A, but had no effect on C29A variants. Evidently, Cys-108 is inaccessible to the bulky 5,5′-dithiobis-2-nitrobenzoate molecule, and inactivation was because of reaction with Cys-29. The smaller alkylating agent iodoacetamide had no effect on any GAT variant.

To identify ionizable groups that are relevant to the catalytic mechanism, we measured the pH dependence of k_{cat} for R7 GAT. As shown in Fig. 3*A*, the pH profile indicates that k_{cat} depends on the ionization of two groups. The first must be deprotonated for activity, and likely corresponds to a catalytic base with a pK value of 5.7. The second must be protonated for activity, and likely corresponds to a catalytic acid with a pK value of 7.5.

Given its sequence conservation (Fig. 1) and its location 5.5 Å from the presumptive position of the nitrogen atom of glyphosate (pK_a of 10.3 (3)) (Fig. 2*C*), His-138 is the most likely amino acid to function as a general base. Replacing His-138 with ala-

nine in R7 GAT caused a 110-fold decrease in k_{cat} relative to the R7 GAT enzyme (Table 4). Substituting alanine for any of the conserved active site arginines, Arg-111, Arg-21 and Arg-73, reduced k_{cat} more modestly, by 26-, 4.3-, and 1.3-fold, respectively.

TABLE 4

Steady-state kinetic data for site-directed mutants constructed in R7 GAT

Values are the means ± S.E. from 3 to 5 separate determinations, each performed in duplicate.

Enzyme	k_{cat}	$K_{m,GPJ}$	$k_{cat}/K_{m,GPJ}$
	min^{-1}	mM	$mM^{-1}\ min^{-1}$
R7	1040 ± 40	0.24 ± 0.01	4330
C108A	1290 ± 20	0.25 ± 0.01	5160
Y118F	60 ± 3	5.2 ± 0.1	11.5
H138A	9.4 ± 0.3	10.6 ± 0.6	0.89
R111A	40 ± 1	61 ± 3	0.66
R21A	240 ± 10	41 ± 4	5.9
R73A	820 ± 20	41 ± 3	20
L20I	1890 ± 40	7.8 ± 0.4	240
T132I	1470 ± 30	0.74 ± 0.04	1990
V135I	2100 ± 90	1.5 ± 0.1	1400
F31Y	1080 ± 40	0.38 ± 0.01	2840
F31Y/V135I	1050 ± 10	1.6 ± 0.06	660
A114V	2100 ± 80	3.2 ± 0.2	660

We also investigated the ability of the conserved active site residue, Tyr-118, to function as a general acid. Tyr-118 makes a direct hydrogen bond (3.3 Å) to the sulfur atom of AcCoA in the crystal structure (Fig. 2*C*), where it is poised to protonate the thiolate anion of the CoA leaving group. Substituting Tyr-118 with phenylalanine in R7 GAT caused a significant (17-fold) decrease in k_{cat} at pH 6.8, and eliminated the basic limb of the k_{cat} *versus* pH profile (Fig. 3*A*). At pH 8.5, where tyrosine is largely in the phenolate form, k_{cat} for R7-Y118F is nearly equivalent to that of R7.

Shuffling Changes—There are a total of 21 amino acid substitutions in R7 GAT resulting in a 200-fold increase in k_{cat} and a 5.4-fold decrease in $K_{m,GPJ}$ relative to the native enzyme (Table 2). This sequence variation is distributed across the entire structure (Fig. 2*D*), with only 4 of the 21 substitutions located within 5 Å of either AcCoA or 3PG (Figs. 1 and 2*C*). To examine the effect of individual shuffling changes on catalysis, we generated four site-directed mutants in which these active site residues (Phe-31, Ala-114, Thr-132, and Val-135) in the R7 enzyme were changed back to the native sequence. Surprisingly, the individual revertants had little impact on k_{cat}, with 3 of the 4 revertants actually showing slight improvement (Table 4). In contrast, A114V (13-fold) and V135I (6.3-fold) showed a significant increase in $K_{m,GPJ}$ relative to R7 GAT. The other two revertants, T132I and F31Y, show more modest increases in $K_{m,GPJ}$ (Table 4). Most significant is that in all cases, the variant residue possesses a smaller side chain than the native residue.

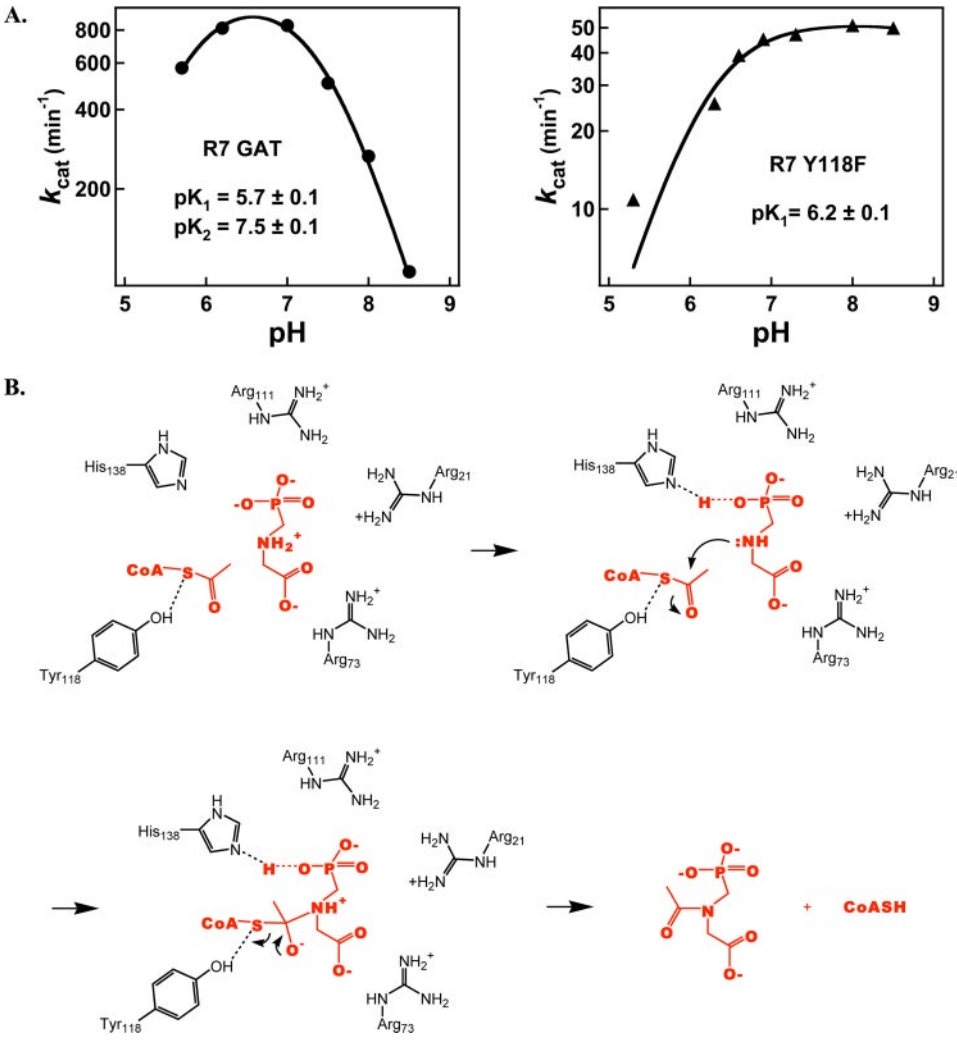

FIGURE 3. *A*, plots of k_{cat} *versus* pH for *N*-acetylation of glyphosate by R7 (●) and R7-Y118F (▲) GAT. The pK_1 and pK_2 values shown on the *graphs* refer to the acidic and basic limbs of the profiles, respectively. See "Experimental Procedures" for experimental conditions and theoretical fits. *B*, proposed chemical mechanism for *N*-acetylation of glyphosate by GAT.

DISCUSSION

Mechanism of Glyphosate N-Acetylation by GAT

The kinetic and structural data presented here allow us to propose a detailed mechanism for glyphosate binding and *N*-acetylation by GAT. The lack of an essential cysteine in the GAT active site, as evidenced by the fully functional C108A mutant, as well as the observed ternary complex structure, suggests that the reaction proceeds via direct acetyl transfer from AcCoA to the secondary amine of glyphosate (Fig. 3*B*), rather than by a ping-pong mechanism involving an acetyl-enzyme intermediate. This general mechanism is used by nearly all known GNAT enzymes (16).

Based on the stereochemical similarity of the compounds, we infer that glyphosate binds in the same location and orientation as 3PG, with its carboxyl group in contact with Arg-73 and Arg-21, and its phosphonyl group in contact with

His-138, Arg-21, and Arg-111. Site-directed alanine mutants implicate each of these residues in glyphosate binding. In particular, alanine substitutions at any of the active site arginines dramatically increase $K_{m,GPJ}$ by 170–250-fold (Table 4).

With a pK_a of 10.3 (3), the glyphosate amine is largely protonated at physiological pH and must be deprotonated prior to acetyl transfer. In GAT, the same basic residues implicated in glyphosate binding also contribute to a positively charged active site (Fig. 2*B*). As proposed in the case of the yeast histone acetyltransferase HpaII (17), this net positive electrostatic potential is likely to lower the pK_a value of the substrate amine upon substrate binding. However, individual alanine substitutions constructed at each of the basic GAT residues reveal significant and differential effects on k_{cat}. Although alanine mutations at any of the active site arginines reduce k_{cat} between 1.3- and 26-fold, mutation of His-138 to alanine results in a 110-fold reduction in k_{cat} (Table 4). A decline of this magnitude is consistent with that expected for loss of a catalytic base (18–20), and it suggests that His-138 plays a specific catalytic role during the reaction.

All GAT variants that we tested, including the three native *B. licheniformis* GAT enzymes (1), contain histidine at position 138 and exhibit an optimal k_{cat} at pH ~ 6.8, as shown for R7 in Fig. 3*A*. The pH-rate analysis of R7 GAT with glyphosate (Fig. 3*A*) suggests the presence of one or more ionizable groups in the enzyme-substrate complex with a pK_1 of 5.7 that must be deprotonated for maximal activity, and we attribute this to His-138 (solution pK_a ~ 6.0) and to the phosphonate group of glyphosate (solution pK_a ~ 5.7).

In the ternary complex His-138 is located 5.5 Å from C-3 of 3PG, the atom corresponding to the nitrogen of glyphosate (Fig. 2*C*). This is too far for His-138 to function directly as a catalytic base. In the true substrate complex subtle differences in the conformation of glyphosate (relative to 3PG) or in the position of His-138 might bring the substrate amine closer to His-138. Alternatively, the specific effect of His-138 on k_{cat} could be mediated by water molecules in the active site, as observed in other members of the GNAT family (15, 16). However, none of the active site waters observed in the crystal structure are located within hydrogen bonding distance of the His-138 side chain.

We favor an alternative mechanism by which His-138 catalyzes substrate deprotonation, shown in Fig. 3*B*. In the crystal structure, determined at pH 4.6, His-138 forms a short 2.46-Å hydrogen bond with one of the phosphate oxygens of 3PG. Similar short hydrogen bonds are observed in the active sites of a number of enzymes, and they are proposed to play a variety of significant roles in catalysis (21–23). At physiological pH, the His-138 side chain and the glyphosate phosphonate group are likely in a deprotonated state. Upon substrate binding we propose that a proton from the secondary amino group of glyphosate is stabilized on a phosphonate oxygen atom, resulting in formation of a strong hydrogen bond between His-138 and glyphosate (Fig. 3*B*) and activation of the substrate amine. This substrate-assisted proton transfer mechanism is consistent with the observed pH dependence of k_{cat} (Fig. 3*A*) and explains the dual role of His-138 in substrate binding and as a catalytic base.

Polarization of the AcCoA carbonyl thioester and stabilization of the tetrahedral intermediate formed after attack by the substrate amine lone pair is typically performed in GNAT enzymes by a pair of main chain amide hydrogens (15, 16). In R7 GAT, the main chain amides of residues Gly-74 and Met-75, part of the structurally conserved β-bulge in β4, are positioned to fulfill this role (Fig. 2*C*).

In some members of the GNAT superfamily an active site residue functions as a general acid to protonate the thiolate anion that forms on CoA upon collapse of the tetrahedral intermediate (15, 16). In GAT, the hydroxyl group of Tyr-118 is located within 3.3 Å of the sulfur atom of CoA, where it is perfectly positioned to perform this function. Mutating Tyr-118 to phenylalanine resulted in an 17-fold drop in k_{cat} at pH 6.8 (Table 4) and eliminated the basic limb of the pH *versus* k_{cat} plot (Fig. 3*A*), suggesting that Tyr-118 should be in the neutral form for optimal GAT activity. Indeed, k_{cat} for R7 at pH 8.5, where Tyr-118 would largely be de-protonated, is nearly the same as for R7-Y118F. The rate acceleration we attribute to Tyr-118 (17-fold) is typical for acid-base catalysts (18) and is similar to that seen in other members of the GNAT superfamily (14, 19).

Substrate Specificity and Optimization for Glyphosate

Substrate Specificity—The physiological role and natural substrates of the bacterial GAT-like enzymes (Fig. 1) are unknown. The most active compound we tested with native GAT is the D-isomer of AP3, a 4-atom (main chain) molecule that is acetylated with a k_{cat}/K_m value of 1500 min^{-1} mM^{-1}. Although it is significantly more active than any of the amino-containing compounds we tested against native GAT, D-AP3 is a relatively poor substrate compared with the substrates of other *N*-acetyltransferases (4, 24–26). Furthermore, although AP3 is a naturally occurring phosphonate, found in *Tetrahymena* and the soft coral *Zoanthus* (27–29), there is no defined physiological role for the D-isomer of AP3.

Analysis of the structure-activity relationship for the series of inhibitors tested against the native and optimized GAT enzymes reveals two general trends as follows: 1) native GAT binds shorter ligands (chiefly 3 and 4 atoms in the main chain) more tightly than longer ones, and 2) progressive optimization for glyphosate activity is accompanied by improved binding to longer ligands (up to ~5 atoms in the main chain) and retained binding to shorter ligands (Table 3). For example, the 3- and 4-atom main chain compounds (*e.g.* 2-phosphonoacetate, phosphonopyruvate, and PEP) are all significantly better inhibitors (K_i ~ 10 μM) of native GAT than are the 5- and 6-atom main chain compounds (K_i values ranging from 140 μM to no measurable inhibition). After optimization for the 5-atom main chain substrate glyphosate, the 5- and 6-atom main chain compounds (*e.g.* NAG, DL-AP4, and DL-AP5) bind more tightly (up to 50-fold) to R11 than to native GAT, whereas the shorter compounds remain potent inhibitors of the native and optimized enzymes.

The active site of GAT dictates not only the acceptable size of a substrate but also its stereochemical configuration. This is best illustrated by AP3. Although the D-isomer is a substrate for each enzyme, the L-isomer is a potent inhibitor of R7 and R11.

Taken together with previous results (4), the structure-activity data indicate a narrow substrate range for native GAT and variants optimized for acetylation of glyphosate. Appreciable activity requires an amine-containing compound with a phosphonyl or phosphoryl and a carboxyl group with a main chain length of 5 or fewer atoms. Of the numerous compounds we tested (Table 3) (4), those that lie outside these parameters all fail to exhibit appreciable activity with native GAT or any variant.

It is interesting to note that the activity for D-AP3 drops by less than 5-fold in R11 relative to the native enzyme, whereas glyphosate activity increases by 4,500-fold. Thus, the original GAT activity against D-AP3 is robust to the large number of changes accumulated in R11 GAT during the course of the optimization for glyphosate. This is consistent with other experiments in which optimization of a weak starting activity is driven by mutations that have little effect on the original (strong) activity but a dramatic effect on the optimized activity (30).

Glyphosate Optimization—The 1100-fold increase in glyphosate *N*-acetylation by R7 GAT is achieved through a combination of improvements in k_{cat} (200-fold) and in $K_{m,GPJ}$ (5.4-fold). There are 21 amino acids differences (out of 146) between R7 GAT and the native enzyme (Fig. 2*D*, *yellow spheres*). Strikingly, none of these changes occur at sites comprising the catalytic machinery. Indeed, only four of the changes are located within 5 Å of the cofactor or 3PG (Fig. 2*D*, *blue spheres*). In almost all of these cases, Y31F, V114A, I132T, and I135V, the optimized enzyme contains a smaller side chain than that present in the native enzyme, consistent with the kinetic data suggesting that GAT is optimized to accommodate a larger substrate, glyphosate.

Single-site revertants constructed at each of the four active site variable positions reveal three that significantly increase $K_{m,GPJ}$ (Table 4). In particular, a 6.2-fold increase in $K_{m,GPJ}$ is observed for the R7-V135I revertant. This substitution alone accounts for the entire 5.4-fold improvement in $K_{m,GPJ}$ observed in the R7 enzyme. The inability of glyphosate to inhibit the glyphosate-insensitive G96A mutant of EPSP synthase from *E. coli* arises from a van der Waals clash between the methyl group of Ala-96 and the phosphonate group of glyphosate (31). In the crystal structure of GAT, Val-135 is in an analogous position, just 3.5 Å from the glyphosate phosphonate group. It appears that gain-of-function substitutions in the optimized R7 GAT serve, in part, to relieve similar steric clashes in the substrate-binding pocket of native GAT.

The present results offer little insight into how the 200-fold increase in k_{cat} was achieved in the optimized R7 enzyme. Single-site revertants constructed at each of the four active site positions reveal minimal effects on k_{cat}. Substitutions located distal to the active site (Fig. 2*D*, *yellow spheres*) may remodel the active site through subtle rearrangements that influence the enzyme structure and flexibility (32–35) to speed up the rate-limiting step of the overall reaction.

The outcome of our optimization experiments with GAT is an enzyme with activity against glyphosate that is comparable with that of other *N*-acetyltransferases for their natural substrates. This includes another herbicide resistance enzyme, phosphinothricin acetyltransferase, which acetylates phosphinothricin (PPT) with a $k_{cat}/K_{m,AcCoA}$ of 6×10^4 M^{-1} s^{-1} and a $k_{cat}/K_{m,PPT}$ of 3×10^5 M^{-1} s^{-1} (4). The k_{cat}/K_m of the R11 GAT enzyme for AcCoA and glyphosate is 2×10^7 and $\sim 5 \times 10^5$ M^{-1} s^{-1}, respectively. In contrast, the diffusion-limited maximal value for k_{cat}/K_m is 10^9 M^{-1} s^{-1} (18). Thus, despite the dramatic improvement in activity with glyphosate, GAT is far from the limits of optimization.

Acknowledgments—We thank John Bedbrook and Michael Lassner for support and for helpful discussions, Y.-H. Chen and J. Gao at Maxygen for mass spectrometric analysis, and Zhenglin Hou and Bill Zimmerman for insightful comments on the manuscript. The Advanced Light Source is supported by the Director, Office of Science, Office of Basic Energy Sciences, of the United States Department of Energy under Contract DE-AC02-05CH11231.

REFERENCES

1. Castle, L. A., Siehl, D. L., Gorton, R., Patten, P. A., Chen, Y. H., Bertain, S., Cho, H. J., Duck, N., Wong, J., Liu, D., and Lassner, M. W. (2004) *Science* **304,** 1151–1154
2. Padgette, S. R., Re, D. B., Barry, G. F., Eichholtz, D. E., Delanny, X., Fuchs, R. L., Kishore, G. M., and Fraley, R. (1995) in *Herbicide-resistant Crops: Agricultural, Economic, Environmental, Regulatory, and Technological Aspects* (Duke, S. O., ed) pp. 53–84, CRC/Lewis Publishers, Boca Raton, FL
3. Franz, J. E., Mao, M. K., and Sikorski, J. A. (1997) *Glyphosate: A Unique Global Herbicide,* American Chemical Society, Washington, D. C.
4. Siehl, D. L., Castle, L. A., Gorton, R., Chen, Y. H., Bertain, S., Cho, H. J., Keenan, R., Liu, D., and Lassner, M. W. (2005) *Pest Manag. Sci.* **61,** 235–240
5. Scopes, R. K. (1994) *Protein Purification: Principles and Practice,* 3rd Ed., pp. 46–47, Springer-Verlag Inc., New York
6. Leslie, A. G. W. (1992) *Joint CCP4 & ESF-EAMCB Newsletter on Protein Crystallography,* No. 26
7. Collaborative Computational Project Number 4 (1994) *Acta Crystallogr. Sect. D. Biol. Crystallogr.* **50,** 760–763
8. Keenan, R. J., Siehl, D. L., Gorton, R., and Castle, L. A. (2005) *Proc. Natl. Acad. Sci. U. S. A.* **102,** 8887–8892
9. Murshudov, G. N., Vagin, A. A., and Dodson, E. J. (1997) *Acta Crystallogr. Sect. D. Biol. Crystallogr.* **53,** 240–255
10. Emsley, P., and Cowtan, K. (2004) *Acta Crystallogr. Sect. D. Biol. Crystallogr.* **60,** 2126–2132
11. DeLano, W. L. (2002) *The PyMOL Molecular Graphics System*, DeLano Scientific LLC, San Carlos, CA
12. Neuwald, A. F., and Landsman, D. (1997) *Trends Biochem. Sci.* **22,** 154–155
13. Wybenga-Groot, L. E., Draker, K., Wright, G. D., and Berghuis, A. M. (1999) *Structure* **7,** 497–507
14. Hickman, A. B., Namboodiri, M. A., Klein, D. C., and Dyda, F. (1999) *Cell* **97,** 361–369
15. Dyda, F., Klein, D. C., and Hickman, A. B. (2000) *Annu. Rev. Biophys. Biomol. Struct.* **29,** 81–103
16. Vetting, M. W., de Carvalho, L. P. S., Yu, M., Hegde, S. S., Magnet, S., Roderick, S. L., and Blanchard, J. S. (2005) *Arch. Biochem. Biophys.* **433,** 212–226
17. Angus-Hill, M. L., Dutnall, R. N., Tafrov, S. T., Sternglanz, R., and Ramakrishnan, V. (1999) *J. Mol. Biol.* **294,** 1311–1325
18. Walsh, C. (1979) *Enzymatic Reaction Mechanisms*, pp. 34 and 42, W. H. Freeman & Co., San Francisco
19. Scheibner, K. A., De Angelis, J., Burley, S. K., and Cole, P. A. (2002) *J. Biol. Chem.* **277,** 18118–18126
20. Tanner, K. G., Trievel, R. C., Kuo, M. H., Howard, R. M., Berger, S. L., Allis, C. D., Marmorstein, R., and Denu, J. M. (1999) *J. Biol. Chem.* **274,** 18157–18160

21. Cleland, W. W. (2000) *Arch. Biochem. Biophys.* **382,** 1–5
22. Kim, K. S., Oh, K. S., and Lee, J. Y. (2000) *Proc. Natl. Acad. Sci. U. S. A.* **97,** 6373–6378
23. Nishina, Y., Sato, K., Tamaoki, H., Tanaka, T., Setoyama, C., Miura, R., and Shiga, K. (2003) *J. Biochem.* (*Tokyo*) **134,** 835–842
24. Draker, K. A., and Wright, G. D. (2004) *Biochemistry* **43,** 446–454
25. Hegde, S. S., Javid-Majd, F., and Blanchard, J. S. (2001) *J. Biol. Chem.* **276,** 45876–45881
26. De Angelis, J., Gastel, J., Klein, D. C., and Cole, P. A. (1998) *J. Biol. Chem.* **273,** 3045–3050
27. Kitteredge, J. S., and Hughes, R. R. (1964) *Biochemistry* **3,** 991–996
28. Smith, J. D., and Law, J. H. (1970) *Biochemistry* **9,** 2152–2157
29. Warren, W. A. (1968) *Biochim. Biophys. Acta* **156,** 340–346
30. Aharoni, A., Gaidukov, L., Khersonsky, O., McQ Gould, S., Roodveldt, C., and Tawfik, D. S. (2005) *Nat. Genet.* **37,** 73–76
31. Eschenburg, S., Healy, M. L., Priestman, M. A., Lushington, G. H., and Schonbrunn, E. (2002) *Planta* **216,** 129–135
32. Benkovic, S. J., and Hammes-Schiffer, S. (2003) *Science* **301,** 1196–1202
33. Oue, S., Okamoto, A., Yano, T., and Kagamiyama, H. (1999) *J. Biol. Chem.* **274,** 2344–2349
34. Piana, S., Carloni, P., and Rothlisberger, U. (2002) *Protein Sci.* **11,** 2393–2402
35. Tomatis, P. E., Rasia, R. M., Segovia, L., and Vila, A. J. (2005) *Proc. Natl. Acad. Sci. U. S. A.* **102,** 13761–13766